Biochemistry

Article

Cite This: *Biochemistry* 2018, 57, 5271−5281

pubs.acs.org/biochemistry

Insights into the Structures of Superoxide Reductases from the Symbionts *Ignicoccus hospitalis* and *Nanoarchaeum equitans*

Célia V. Romão,[*,†] Pedro M. Matias,[†,‡] Cristiana M. Sousa,[‡] Filipa G. Pinho,[‡] Ana F. Pinto,[†] Miguel Teixeira,[*,†] and Tiago M. Bandeiras[*,†,‡]

[†]ITQB NOVA, Instituto de Tecnologia Química e Biológica António Xavier, Universidade Nova de Lisboa, Av. da República, 2780-157 Oeiras, Portugal

[‡]iBET, Instituto de Biologia Experimental e Tecnológica, Apartado 12, 2781-901 Oeiras, Portugal

ABSTRACT: Superoxide reductases (SORs) are enzymes that detoxify the superoxide anion through its reduction to hydrogen peroxide and exist in both prokaryotes and eukaryotes. The substrate is transformed at an iron catalytic center, pentacoordinated in the ferrous state by four histidines and one cysteine. SORs have a highly conserved motif, (E)(K)HxP-, in which the glutamate is associated with a redox-driven structural change, completing the octahedral coordination of the iron in the ferric state, whereas the lysine may be responsible for stabilization and donation of a proton to catalytic intermediates. We aimed to understand at the structural level the role of these two residues, by determining the X-ray structures of the SORs from the hyperthermophilic archaea *Ignicoccus hospitalis* and *Nanoarchaeum equitans* that lack the quasi-conserved lysine and glutamate, respectively, but have catalytic rate constants similar to those of the canonical enzymes, as we previously demonstrated. Furthermore, we have determined the crystal structure of the E23A mutant of *I. hospitalis* SOR, which mimics several enzymes that lack both residues. The structures revealed distinct structural arrangements of the catalytic center that simulate several catalytic cycle intermediates, namely, the reduced and the oxidized forms, and the glutamate-free and deprotonated ferric forms. Moreover, the structure of the *I. hospitalis* SOR provides evidence for the presence of an alternative lysine close to the iron center in the reduced state that may be a functional substitute for the "canonical" lysine.

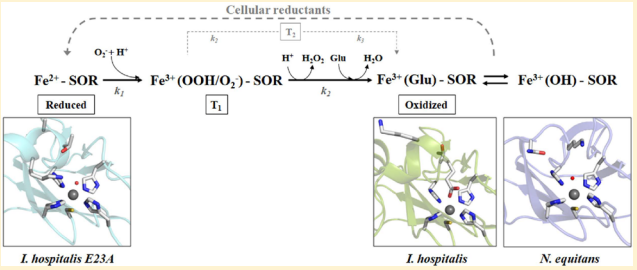

Superoxide reductases (SORs) are enzymes involved in the detoxification of the superoxide anion ($O_2^{\bullet-}$), via its reduction to hydrogen peroxide (for reviews, see refs 1−5). Although the first SORs described were from anaerobic and microaerophilic prokaryotes,[1,6−8] today it is known that these enzymes are widespread in organisms from the three domains of life, including aerobic eukaryotes, such as *Phaeodactylum tricornutum* and *Monosiga brevicollis*.[9]

All SORs share the same catalytic domain, in which the iron in the active site is pentacoordinated by five strictly conserved residues: four equatorial histidine-imidazoles and one axial cysteine-sulfur in a square pyramidal geometry [Fe(Cys)-$(His)_4$]. Apart from these ligands, two other highly conserved residues have been proposed to be involved in the overall catalytic mechanism, a glutamate and a lysine, in the -(E)(K)HxP- motif, in which the histidine is one of the conserved ligands.

All the SOR crystal structures so far determined can be divided into "closed" and "open" conformations, in relation to access to the iron center. In the crystal structures of the SORs from the archaea *Pyrococcus furiosus*[10] and *Pyrococcus horikoshii* [Protein Data Bank (PDB) entry 2HVB] and from the eukaryote *Giardia intestinalis*,[11] the glutamate is bound to the ferric ion, on what may be considered a "closed conformation", corresponding to the oxidized state, as shown by Fourier transform infrared spectroscopy (FTIR) studies.[12,13] In all remaining structures, presumably from the ferrous state, the glutamate is displaced from the iron ion, while the lysine is ∼7.4 Å from it but not bound to it.[14−16] Under these conditions, several anions were observed to bind to the iron center, such as chloride, ferricyanide, nitrate, or peroxo ions.[14,15] The common feature among them is the position of the lysine residue that is always at the top of the iron center, on what may be considered an "open conformation", in the sense that the sixth axial position is more accessible to bind the substrate for the inner-sphere electron transfer reaction.

X-ray and FTIR studies showed that the glutamate is involved in a redox-linked conformational change, upon reduction of the ferric iron, being detached from the metal ion with a concomitant movement of a loop that contains the glutamate and lysine residues.[10,12,13] Simultaneously, the lysine, which is ∼12 Å from the metal in the ferric form, approaches the reduced metal ion. This residue has been proposed to contribute to attracting the anionic substrate by increasing the positive surface charge around the catalytic site[17] and providing the proton to the superoxo/hydroperoxo

Received: March 20, 2018
Revised: May 22, 2018
Published: June 25, 2018

DOI: 10.1021/acs.biochem.8b00334
Biochemistry 2018, 57, 5271−5281

Table 1. Data Collection and Processing Statistics[a]

	I. hospitalis SOR wild type	*I. hospitalis* SOR E23A	*N. equitans* SOR
beamline	ESRF, ID23-1	in house	ESRF, ID23-1
wavelength (Å)	0.9800	1.5418	0.9793
space group	$P6_222$ or $P6_422$	$P2_1$	$P2_12_12_1$
unit cell parameters	a = 108.7 Å, c = 61.4 Å	a = 54.9 Å, b = 74.8 Å, c = 68.8 Å, β = 106.7°	a = 51.88 Å, b = 82.01 Å, c = 91.30 Å
resolution range (Å)	50.0−1.85 (1.89−1.85)	40.7−2.05 (2.11−2.05)	45.1−1.88 (1.95−1.88)
scan type	φ	Ω	φ
total angular range (deg)	100.0	450.5	107
total no. of frames	200	1802	214
exposure time per frame (s)	0.8	20	0.1
no. of observations	217242 (12198)	123294 (6291)	129895 (8825)
no. of unique reflections	18720 (1088)	33545 (2615)	31984 (2864)
$\langle I/\sigma(I)\rangle$	17.8 (1.6)	11.4 (2.3)	14.1 (2.6)
R_{merge} (%)[b]	7.1 (130.7)	6.5 (51.2)	5.4 (38.3)
R_{meas} (%)[c]	7.4 (137.0)	7.5 (64.8)	6.2 (45.3)
R_{pim} (%)[d]	2.1 (39.8)	3.6 (39.2)	3.0 (23.7)
completeness (%)	99.1 (95.4)	99.9 (99.4)	98.6 (91.6)
multiplicity	11.6 (11.2)	3.7 (2.4)	4.1 (3.1)
$CC_{1/2}$	0.999 (0.725)	0.997(0.784)	0.998 (0.858)
Wilson B-factor (Å^2)	35.6	33.2	28
no. of molecules in the asymmetric unit	1	4	4
V_m (Å^3 Da^{-1})	3.8	2.4	1.9
estimated solvent content (%)	67.3	49.1	36

[a]Values in parentheses are for the highest-resolution shell. [b]Merging R-factor, $R_{merge} = [\sum_{hkl}\sum_i|I_i(hkl) - \langle I(hkl)\rangle|]/[\sum_{hkl}\sum_i I(hkl)] \times 100\%$, where $I_i(hkl)$ is the intensity measured for each unique Bragg reflection with indices (hkl) and $\langle I(hkl)\rangle$ is the average intensity for multiple measurements of this reflection. [c]Multiplicity-independent R-factor, $R_{meas} = \sum_{hkl}[N_{hkl}/(N_{hkl} - 1)]^{1/2}\sum_i|I_i(hkl) - \langle I(hkl)\rangle|/[\sum_{hkl}\sum_i I(hkl)] \times 100\%$. [d]Precision-independent R-factor, $R_{pim} = \sum_{hkl}[1/(N_{hkl} - 1)]^{1/2}\sum_i|I_i(hkl) - \langle I(hkl)\rangle|/\sum_i I_i(hkl) \times 100\%$, where $I_i(hkl)$ is the observed intensity, $\langle I(hkl)\rangle$ is the average intensity of multiple observations from symmetry-related reflections, and N_{hkl} is their multiplicity.[69]

intermediate, directly or through a chain involving water molecules, to generate the product, H_2O_2.[15,18,19]

The function of these two residues has been addressed by enzymatic studies of several SOR site-directed mutants,[17,20−22] and of "natural" mutants, i.e., SORs lacking either the glutamate (from *Nanoarchaeum equitans*[23]) or the lysine (from *Ignicoccus hospitalis*[24]). These studies showed that *in vitro* the absence of the glutamate does not have any consequence in catalysis, while the mutation of the lysine led to a decrease in the rate constant for the formation of the first catalytic intermediate, from 1×10^9 M^{-1} s^{-1} for the wild-type enzyme to 4.2×10^7 M^{-1} s^{-1} for the lysine mutant. Furthermore, the *Desulfoarculus baarsii* SOR K48I mutant exhibited new properties, being capable of a two-electron oxidation of organic substrates in the presence of H_2O_2, through the formation of an oxoferryl [Fe(IV)=O] species, which was not observed for the wild-type enzyme.[3,22] However, this result contrasts with the behavior of the wild-type *I. hospitalis* SOR, which exhibits a rate constant of 0.7×10^9 M^{-1} s^{-1} for the reaction with superoxide, a value very similar to those of the canonical enzymes ($\sim 10^9$ M^{-1} s^{-1})[24] regardless of its natural lack of the lysine mentioned above.

Therefore, the question that remains to be answered for these "natural mutants" is whether there are structurally equivalent amino acids that functionally would replace those residues. To address this question, we decided to structurally study two 1Fe-SORs, from *I. hospitalis* [(-E_{23}T)HxP$_{27}$- motif] and *N. equitans* [(-P_8K)HxP$_{12}$- motif], which lack those lysine and glutamate residues and have been kinetically characterized.[23,24] These SORs represent excellent targets for structurally analyzing the catalytic center environment in the absence of these two residues. These organisms are anaerobic hyperthermophilic archaea isolated from a submarine hydrothermal system at the Kølbeinsey Ridge (north of Iceland)[25] and are the only known archaeal host−symbiont system. It is interesting to note that they do not contain genes encoding the canonical superoxide detoxifying enzyme superoxide dismutase, having to rely only on the SORs for superoxide detoxification.

Here, the SOR crystal structures for the wild-type proteins from *I. hospitalis* and *N. equitans* were determined, as well as the crystal structure of the *I. hospitalis* SOR mutant E23A, which lacks the glutamate, therefore mimicking the structures of several putative SORs from Eukarya that lack both amino acids.[9,24] Furthermore, the obtained data allowed us to propose structures for the catalytic intermediates of the SORs and reveal an alternative lysine residue that may fulfill the same role as the "canonical" lysine of the -(E)(K)HxP- motif.

MATERIALS AND METHODS

Protein Purification. The recombinant proteins were expressed and purified as previously described.[23,24] The final conditions for each purified protein sample were at concentration of 15 mg/mL in 20 mM Tris-HCl (pH 7.2) and 150 mM NaCl for the *I. hospitalis* SORs (wild type and E23A variant) and a concentration of 30 mg/mL in 20 mM Tris-HCl (pH 7.2) and 150 mM NaCl for wild-type *N. equitans* SOR. The protein purity was assessed by sodium dodecyl sulfate−polyacrylamide gel electrophoresis and ultraviolet−visible spectroscopy.

Crystallization and Cryoprotection. Crystallization trials were performed on the nanoliter scale with the Classic Screen (Nextal) using a Cartesian Crystallization Robot Dispensing System (Genomics Solutions) and round-bottom Greiner 96-

DOI: 10.1021/acs.biochem.8b00334
Biochemistry 2018, 57, 5271−5281

Table 2. Structure Refinement Statistics[a]

	I. hospitalis SOR	*I. hospitalis* SOR E23A	*N. equitans* SOR
resolution limits (Å)	47.20−1.85 (1.94−1.85)	29.6−2.05 (2.12−2.05)	45.11−1.90 (1.96−1.90)
R-factor[b]	0.180 (0.290)	0.177 (0.275)	0.206 (0.321)
no. of reflections[c]	17747 (2444)	29333 (2362)	29474 (2503)
R_{free}[d]	0.200 (0.300)	0.200 (0.329)	0.240 (0.349)
no. of reflections[c]	968 (145)	1561 (126)	1580 (125)
overall coordinate error estimate (Å)[e]	0.14	0.21	0.27
model completeness and composition			
no. of molecules in the asymmetric unit	1	4	4
no. of non-hydrogen protein atoms	1092	3989	3600
no. of iron ions	1	4	4
no. of solvent molecules	102	139	115
mean *B* values (Å^2)[f]			
protein main chain	38.9	44.4	45.9
protein side chain	44.8	49.9	51.3
ions and ligands	36.2	42.8	46.4
solvent molecules	53.7	42.5	44.3
model root-mean-square deviation from ideality			
bond lengths (Å)	0.007	0.007	0.002
bond angles (deg)	1.051	1.132	0.501
chiral centers (Å^3)	0.080	0.084	0.051
planar groups (Å)	0.006	0.005	0.004
model validation[g]			
% Ramachandran outliers	0	0	0
% Ramachandran favored	98.4	97.8	98.1
% rotamer outliers	1.9	3.6	0.26
C^β outliers	0	0	0
Clash score	4.1	6.9	4.3
PDB entry	4BK8	4BRV	6GQ8

[a]Values in parentheses are for the highest-resolution shell. [b]*R*-factor = $\sum_{hkl}||F_o| - |F_c||/\sum_{hkl}|F_o|$, where $|F_o|$ and $|F_c|$ are the observed and calculated structure factor amplitudes, respectively. [c]No $\sigma(F_o)$ cutoff. [d]Cross-validation *R*-factor computed from a randomly chosen subset of 5% of the total number of reflections that were not used in the refinement. [e]Maximum-likelihood estimate. [f]Calculated from isotropic or equivalent isotropic *B* values. [g]Calculated with MOLPROBITY.[45]

well CrystalQuick plates (Greiner Bio-One). Crystal optimization was performed by the sitting-drop vapor diffusion technique. Drops (2 μL) were set up at 20 °C in an XRL 24-well crystallization plate (Molecular Dimensions), by mixing the protein solutions with their respective crystallization solutions varying the ratio of protein to reservoir solution, and equilibrated against 500 μL of the crystallization solution in the reservoir. The crystallization condition for wild-type *I. hospitalis* and *N. equitans* SORs and the cryoprotection solution were previously described.[26,27] The E23A *I. hospitalis* SOR mutant that crystallized in 100 mM Tris-HCl (pH 8.5), 10 mM $NiCl_2$, and 20% (w/v) PEG 2000 monomethyl ether (MME) did not require a cryoprotection solution because data were collected in house at room temperature.

Data Collection and Processing. *Wild-Type and E23A I. hospitalis SORs.* An initial low-resolution model (2.4 Å) of wild-type SOR from *I. hospitalis* was built from diffraction data collected in house at room temperature using a Bruker AXS Proteum Pt135 CCD detector system coupled to a Bruker AXS Microstar-I rotating-anode X-ray generator with Montel mirrors as previously described.[27] Subsequently, a 1.85 Å resolution diffraction data set was collected at 100 K from a wild-type *I. hospitalis* SOR crystal, at beamline ID23-1 of the European Synchrotron Radiation Facility (ESRF) in Grenoble, France. Finally, a 2.05 Å data set was measured in house at room temperature for the E23A *I. hospitalis* SOR crystal.

The images obtained at the synchrotron beamline were integrated and scaled with the XDS program package.[28] The images collected in house were processed with SAINT and scaled using SADABS as part of the Bruker AXS Proteum software suite. The diffraction intensities were subsequently merged with SCALA and converted to structure factors with CTRUNCATE in the CCP4 suite.[29]

Wild-Type N. equitans SOR. Diffraction data from a flash-cooled crystal of SOR from *N. equitans* were collected to 1.88 Å resolution at ESRF beamline ID23-1.[26] The diffraction images were integrated with XDS[28] and the resulting intensities subsequently merged with SCALA and converted to structure factors with CTRUNCATE in the CCP4 suite[29] as previously described.[26]

The data collection and processing statistics of the SOR data sets are listed in Table 1.

Structure Determination and Refinement. *Wild-Type and E23A I. hospitalis SORs.* The structure of the wild-type *I. hospitalis* SOR was determined from the 2.4 Å data set measured in house by the single-wavelength anomalous dispersion method using the iron present.[27]

Using the HKL2MAP graphical interface[30] and the SHELXC/D/E program suite,[31−33] the data set was scaled and analyzed with SHELXC, the iron substructure determined with SHELXD, and the phase problem solved with SHELXE. The best solution from SHELXD in 100 trials gave one iron site with a correlation coefficient of 39.9%, and the SHELXE

DOI: 10.1021/acs.biochem.8b00334
Biochemistry 2018, 57, 5271−5281

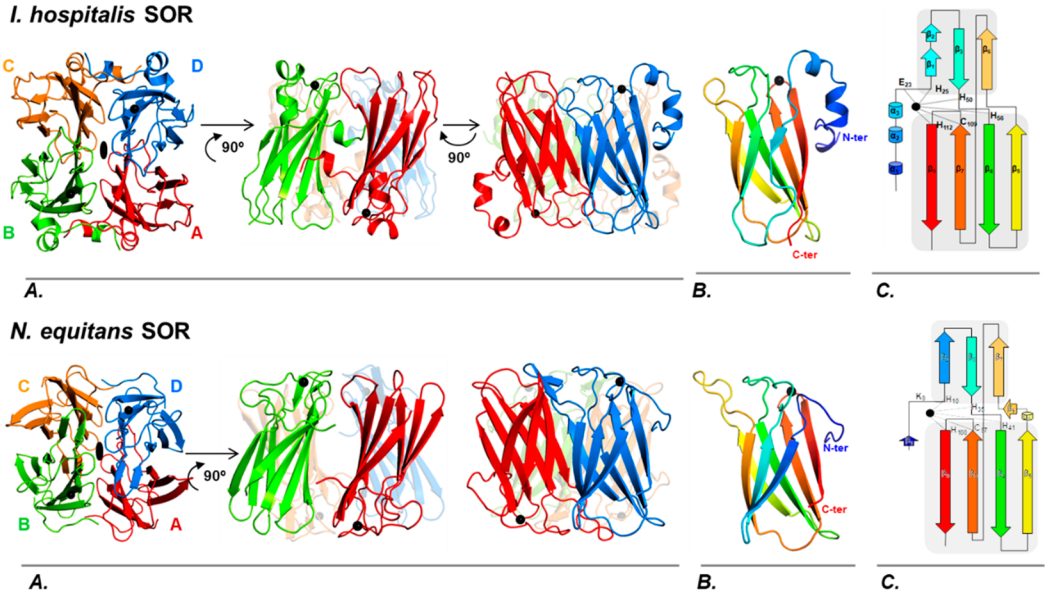

Figure 1. Overall structures of *I. hospitalis* and *N.equitans* SORs. (A) Three different orientations of the tetramer are represented. (B) Monomer representation rainbow-colored from the N-terminus (blue) to the C-terminus (red). (C) Topology diagram of the monomer, colored as in panel B. Each monomer is represented as a cartoon with a different color by chain (A in red, B in green, C in orange, and D in blue), and the iron atoms are represented as black spheres.

calculations gave a clear discrimination between the correct and inverted substructure solutions. The phases derived from the SAD data were improved using the maximum-likelihood heavy-atom parameter refinement in autoSHARP,[34] and a subsequent optimizing density modification procedure using SOLOMON[35] suggested a solvent content of 61.7% and one monomer in the asymmetric unit. Centroid SHARP phases were further improved by density modification with DM.[36] A random 5% sample of the reflection data was used for R_{free} calculations[37] during model building and refinement. Using the 2.4 Å density-modified phases from SOLOMON/DM, 119 of the expected 124 protein residues in the asymmetric unit were built and sequenced automatically with Buccaneer/REFMAC,[38−40] leading to final *R*-factor and R_{free} values of 25.3 and 27.6%, respectively, and the model was completed using COOT.[41] Subsequently, the high-resolution *I. hospitalis* SOR wild-type and E23A protein crystal structures were determined by molecular replacement with PHASER[42] as implemented in the CCP4 suite,[29] using the preliminary structure obtained from the 2.4 Å data as a phasing model.

The *I. hospitalis* SOR structures were refined with PHENIX.[43] During refinement, the models were periodically inspected and corrected with COOT[41] against σ_A-weighted 2|F_o| − |F_c| and |F_o| − |F_c| electron density maps. The solvent molecules were included both by PHENIX and by manual inspection of the electron density maps using COOT.[41] The final refinement cycles included a refinement with a TLS (translation−libration−screw) rigid body refinement of atomic displacement parameters.[44] The model quality was assessed with MolProbity,[45] revealing no outliers in a Ramachandran φ and ϕ plot.[46]

Wild-Type N. equitans SOR. The *N. equitans* SOR crystal structure was determined by the molecular replacement method using PHASER[42] as implemented in PHENIX.[43] One monomer from the *P. furiosus* SOR (PDB entry 1DQI)[10] was used as the search model. Prior to the molecular replacement calculations, it was edited with SCULPTOR, based on a CLUSTALX[47] sequence alignment. The resulting model from PHASER[42] was rebuilt with AUTOBUILD, yielding a continuous model comprising residues Lys9−Leu109. The structure was refined to 1.9 Å resolution with PHENIX using TLS rigid body refinement of atomic displacement parameters, followed by refinement of individual atomic parameters. Five rigid body segments were considered for each of the four monomers in the asymmetric unit, chosen using the TLSMD server[48,49] from the analysis of chain A from an earlier refinement with isotropic refinement of the thermal motion parameters. Noncrystallographic symmetry restraints among the four independent monomers in the asymmetric unit were also applied. Throughout the refinement, the model was periodically checked and corrected with COOT[41] against σ_A-weighted 2|F_o| − |F_c| and |F_o| − |F_c| electron density maps. The solvent molecules were included in the refinement, located by the AUTOBUILD procedure and by inspection of the σ_A-weighted |F_o| − |F_c| electron density maps. The structure was analyzed with MOLPROBITY,[45] and there were no outliers in a Ramachandran φ and ϕ plot.[46]

Details of the overall refinement statistics and final quality of the models for *I. hospitalis* and *N. equitans* SORs are listed in Table 2.

Amino Acid Sequence Alignments. Two independent groups of SOR crystal structures were superimposed using Modeler[50] based on their structural classification as 1Fe- or 2Fe-SORs. Then, ClustalX[47] in Profile Alignment Mode was used to match 1Fe-SOR and 2Fe-SOR sequences, and the alignment was readjusted with Genedoc.[51]

Figures. Figures were prepared with Pymol.[52,53]

Accession Numbers. The coordinates and structure factors have been submitted to the Protein Data Bank in Europe[54,55] as entries 4BK8 and 4BRV for wild-type *I. hospitalis* SOR and its E23A mutant, respectively, and 6GQ8 for *N. equitans* SOR (Table 2).

DOI: 10.1021/acs.biochem.8b00334
Biochemistry 2018, 57, 5271−5281

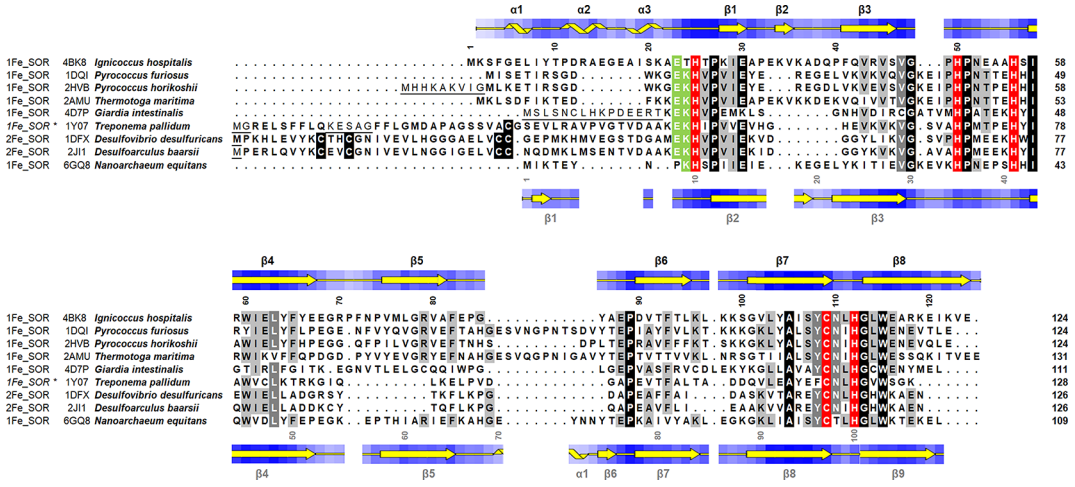

Figure 2. Amino acid sequence alignment of superoxide reductase proteins. Alignment based on three-dimensional structural superpositions of 1Fe-SOR and 2Fe-SORs. The *I. hospitalis* and *N. equitans* SOR secondary structure and amino acid residue relative solvent accessibility distribution (white to blue shading) are shown above and below the alignment, respectively. The different α-helices and β-chains are numbered according to Figure 1. Amino acid residues that coordinate catalytic iron atoms are colored red; the canonical glutamate and lysine residues are colored green. Black boxes denote the strictly conserved residues, dark gray boxes mostly conserved residues, and light gray boxes less conserved residues among the selected sequences. The proteins selected were those for which crystal structures have been deposited, besides those from this work: 1Fe-SOR, *P. furiosus* (PDB entry 1DQI), *P. horikoshii* (PDB entry 2HVB), *G. intestinalis* (PDB entry 4D7P), and *Thermotoga maritima* (PDB entry 2AMU); 2Fe-SOR, *Desulfovibrio desulfuricans* ATCC 27774 (PDB entry 1DFX) and *D. baarsii* (PDB entry 2JI1); 1Fe-SOR*, 1Fe-class III *Treponema pallidum* SOR (PDB entry 1Y07).

RESULTS AND DISCUSSION

Structure Determination and Quality. The crystal structures of the SORs from *I. hospitalis* and *N. equitans* were determined and refined, both to a resolution of ~1.9 Å, in space groups $P6_422$ and $P2_12_12_1$, respectively. Furthermore, the crystal structure of the E23A *I. hospitalis* SOR mutant was determined at a resolution of 2.5 Å in space group $P2_1$. The overall statistics regarding data processing and refinement are listed in Tables 1 and 2.

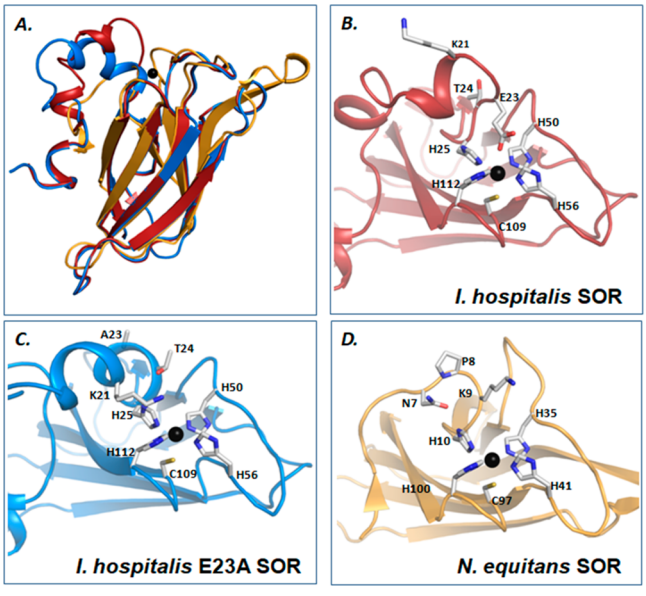

Figure 3. Catalytic iron site of *I. hospitalis* and *N. equitans* SORs. (A) Superposition of the monomers from wild-type *I. hospitalis* SOR (red), E23A *I. hospitalis* SOR (blue), and *N. equitans* SOR (orange). Structures of the iron active centers of (B) wild-type *I. hospitalis* SOR, (C) E23A *I. hospitalis* SOR, and (D) *N. equitans* SOR. Each monomer is represented as a cartoon, with the side chains of the amino acid residues coordinating the iron atom depicted as sticks and the iron atoms shown as black spheres.

The electron density maps (when contoured at the map 1.0σ level) are mostly well-defined for all three crystal structures. The wild-type *I. hospitalis* SOR structure has one molecule in the asymmetric unit (a.u.), and the first methionine was the only amino acid residue that could not be modeled. In the E23A *I. hospitalis* SOR crystal structure, which has four molecules in the a.u., the amino acid residues between positions 13 and 19 were not completely defined, possibly because they are in a very flexible region. This is more evident in chain C, in which the residue's side chains were refined with 50% occupancy, because of the poor electron density. This region corresponds to the loop that has a different conformation between E23A *I. hospitalis* SOR and the wild-type enzyme, which will be discussed below. For the *N. equitans* SOR structure, with four molecules in the a.u., the side chains of residues 31−34, which correspond to the loop between strands β_3 and β_4, are also not well-defined on the electron density maps, possibly because of the high flexibility of this protein region.

SOR Overall Structure. The overall monomer structures and oligomeric organizations of all the proteins are similar to each other and those of other 1Fe-SORs previously structurally characterized.[10,11] The packing of symmetry-related subunits in the crystal structure reveals a tetrameric quaternary structure for all the proteins (Figure 1), in agreement with the biochemical studies.[23,24] The SOR tetramer has a cubically shaped form with point-group symmetry 222 (Figure 1, I). The root-mean-square deviation (rmsd) between the wild-type *I. hospitalis* SOR tetramer and its E23A mutant is 0.8 Å, and it is 1.2 Å for the *N. equitans* SOR tetramer. Surface analysis, determined using PISA,[56] indicates that the *I. hospitalis* SOR tetramer has a larger surface area, ~20010 Å^2, when compared with the *N. equitans* SOR surface, 16150 Å^2 (Figure 1, I), which is mainly because the *I. hospitalis* SOR primary structure

DOI: 10.1021/acs.biochem.8b00334
Biochemistry 2018, 57, 5271−5281

Table 3. Distances between the Iron and the Different Coordinating Amino Acid Residues[a]

	I. hospitalis SOR						*N. equitans* SOR			
	wild type	E23A					wild type			
	Fe	Fe^A	Fe^B	Fe^C	Fe^D		Fe^A	Fe^B	Fe^C	Fe^D
His25 $N^{\varepsilon 2}$	2.17	2.22	2.13	2.19	2.04	His10 $N^{\varepsilon 2}$	2.34	2.25	2.23	2.27
His50 $N^{\varepsilon 2}$	2.25	2.24	2.20	2.28	2.30	His35 $N^{\varepsilon 2}$	2.19	2.26	2.17	2.45
His56 $N^{\varepsilon 2}$	2.20	2.19	2.31	2.22	2.31	His41 $N^{\varepsilon 2}$	2.38	2.22	2.40	2.24
His112 $N^{\delta 1}$	2.20	2.26	2.31	2.17	2.20	His100 $N^{\delta 1}$	2.33	2.40	2.26	2.23
Cys109 S^{γ}	2.37	2.62	2.51	2.57	2.54	Cys97 S^{γ}	2.54	2.43	2.44	2.40
Glu23 $O^{\varepsilon 2}$	2.47									
Lys21 N^{ζ}	–	W1	W2/3	W4	W5	Lys9 N^{ζ}	7.45	7.67	W6	7.12

[a]*I. hospitalis* SOR numbering: His25, His50, His56, His112, Cys109, and Glu23; *N. equitans* SOR numbering: His10, His35, His41, His100, and Cys97. In the crystal structure of E23A *I. hospitalis* SOR, solvent molecules were observed in the four molecules in the a.u. between the iron and Lys21 labeled as W1, W2/3, W4, and W5, and the distances are as follows: W1, Fe···2.24 Å···W1···2.80 Å···Lys21 N^{ζ}; W2/3, Fe···2.35 Å···W2···2.53 Å···W3···2.72 Å Lys21 N^{ζ}; W4, Fe···2.14 Å···W4···5.34 Å···Lys21 N^{ζ}; W5, Fe···2.42 Å···W5···4.96 Å···Lys21 N^{ζ}. In the crystal structure of *N. equitans* SOR, a solvent molecule labeled W6 was observed between the iron and Lys9 in one of the four molecules in the a.u. with the following distances: Fe···2.64 Å···W6···4.78 Å···Lys9 N^{ζ}.

has a longer N-terminus (which nevertheless is quite distinct from those of 1Fe-class III SORs[4]).

Several hydrogen bonds between the different monomers contribute to stabilize the tetramer; however, the intersubunit interactions, determined using HBPLUS,[57] represent only ∼11−17% of the total hydrogen bonds in the tetramer (48 of 428 for *I. hospitalis* SOR and 66 of 381 for *N. equitans* SOR). From those, the main contribution is between subunits A and D and subunits B and C (Figure 1, I), which correspond to 7−10% of the intersubunit hydrogen bonds, while for the AB and DC subunit interactions, the contribution is only 4−5%. Hydrogen bonds between subunit pairs AC and BD are absent in *I. hospitalis* SOR and in *N. equitans* SOR represent only 3% of the total hydrogen bonds. The hydrogen bonds between ionic pairs contribute 37% (25 of 68) and 44% (28 of 64) to the total number of hydrogen bonds between side chains (∼16% of the total hydrogen bonds) in *I. hospitalis* and *N. equitans* SORs, respectively.

SOR Monomer Structure. The structural core of these proteins is a seven-stranded antiparallel β-barrel (3 + 4) with an immunoglobulin-like β-sandwich fold. The secondary structures of *I. hospitalis* and *N. equitans* SORs show that the β-strands within this domain are organized as (β_1:β_2), β_3, β_6 and β_5, β_4, β_7, β_8 for *I. hospitalis* SOR and β_2, β_3, β_7 and β_5, β_4, β_8, β_9 for *N. equitans* SOR (Figures 1, B and C, and 2).

Prior to the first β-strand (β_1) in their β-barrel, *I. hospitalis* SORs have a 27-amino acid residue N-terminal region, which faces the solvent. In this region, the *I. hospitalis* wild-type protein has three helices (α_1−α_3), of which α_3 is of the 3_{10} type. The crystal structure of E23A *I. hospitalis* SOR has four molecules in the asymmetric unit, and the number and type of helices in the N-terminus vary among the different subunits: subunit A, four helices (3_{10}, 3_{10}, 3_{10}, and α); subunit B, three helices (3_{10}, 3_{10}, and α); subunit C, three helices (α, 3_{10}, and α); and subunit D, three helices (α, α, and α). The variation in the number and type of the N-terminal helices in the *I. hospitalis* SOR crystal structures indicates that this region is flexible. In contrast, the N-terminal region of *N. equitans* SOR has only 11 amino acid residues, comprising a short two-residue β-strand (β_1) (Figures 1, B and C, and 2). Furthermore, in *N. equitans* SOR, the region between sheets β_5 and β_6 (amino acid residues 66−77) in subunits A−C contains a 3_{10}-type helix (α_1, residues 70−72), while in subunit D, a loop is observed instead, meaning that this region may adopt helical or coil secondary structures.

Comparison of the SOR monomer structures from this work (Figures 2 and 3) with all the SOR structures available to date shows that the structural core comprising the seven-stranded antiparallel β-barrel is highly conserved, and the main variability occurs in the N-terminal region, which interestingly contains the glutamate and lysine residues of the -(E)(K)HxP- motif; the flexibility of this N-terminal region is probably relevant for the catalytic mechanism, allowing the glutamate or the lysine to be closer to or farther from the iron center, depending on the catalytic state (discussed below). The rmsd of *I. hospitalis* and *N. equitans* SORs between Cα atoms for the other 1Fe-SORs is 1.2 ± 0.2 Å, while for the 2Fe-SORs, the rmsd is ∼1.7 ± 0.5 Å.

Iron Center in the SOR Structures. The catalytic iron center is located within the β-barrel loops and is exposed to the solvent (Figures 1 and 3). The iron is coordinated by four histidine-imidazoles in the equatorial plane and a cysteine-sulfur in one of the axial positions. Distances among the iron, its ligand atoms, and solvent bridge molecules are listed in Table 3. For *I. hospitalis* SORs, the coordinating ligands are His25, His50, His56, His112, and Cys109, and for *N. equitans* SOR, they are His10, His35, His41, His100, and Cys97 (Figure 3). As in other SORs, three of the histidines are coordinated through their $N^{\varepsilon 2}$ atom, while His112 (*I. hospitalis* SOR) and His100 (*N. equitans* SOR) bind through their $N^{\delta 1}$ atom (Figure 3). The wild-type *I. hospitalis* SOR has residue Glu23 as an additional axial ligand to the iron (Figure 3). This residue is in a position structurally similar to those of Glu14 in *P. furiosus* SOR (PDB entry 1DO6),[10] Glu23 in *P. horikoshii* (PDB entry 2HVB), and Glu17 in *G. intestinalis* SOR,[11] which correspond to the "closed conformations", of the oxidized states (Figure 4A). *N. equitans* SOR is a "natural" mutant for the glutamate ligand, having a proline (Pro8) in the equivalent sequence position. Therefore, the second axial coordination position is free or occupied by a solvent species; however, the canonical lysine residue (Lys9) is near the iron center, at a distance of ∼7.4 Å (Figure 3 and Table 3). On all four molecules in the asymmetric unit of the *N. equitans* SOR, the 2|F_o| − |F_c| electron density for the Lys9 side chain is not well-defined at the 1.0σ contour level. However, a lower contour level of the 2|F_o| − |F_c| electron density map shows that this residue is pointing toward the iron. This Lys9 is in a position

DOI: 10.1021/acs.biochem.8b00334
Biochemistry 2018, 57, 5271−5281

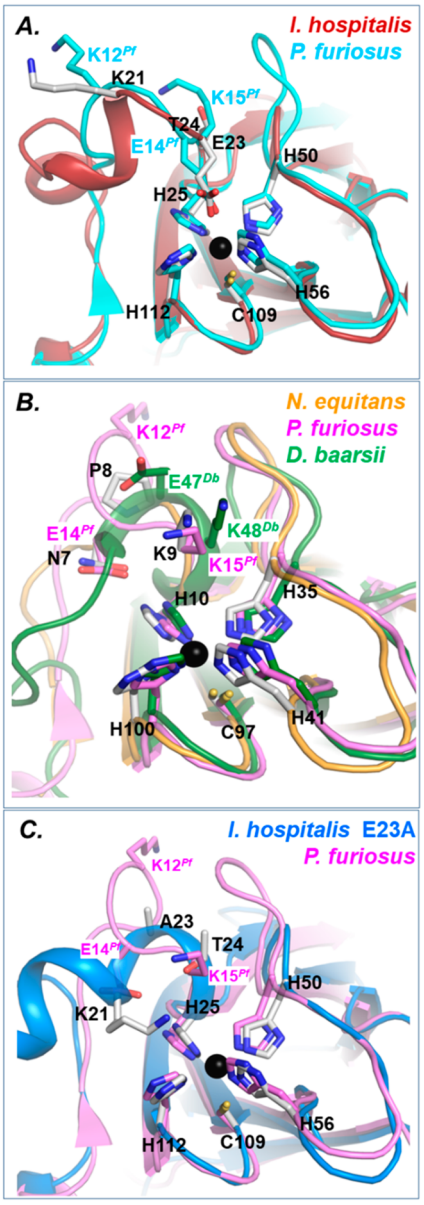

Figure 4. Superposition of SOR iron centers. (A) Active center of *I. hospitalis* SOR (red) superimposed with the corresponding center of 1Fe-SOR from *P. furiosus* (PDB entry 1DO6, chain A) (cyan). (B) Active center of *N. equitans* SOR (orange) superimposed with the 1Fe-SOR from *P. furiosus* (PDB entry 1DQK, chain C) (pink) and with 2Fe-SOR from *D. baarsii* (PDB entry 2JI1, chain A) (green). (C) Active center of E23A *I. hospitalis* SOR (blue) superimposed with the *P. furiosus* 1Fe-SOR (PDB entry 1DQK, chain C) (pink). Monomers are drawn as cartoons, the side chains of the amino acid residues coordinating the iron atom depicted as sticks, and the iron atoms shown as black spheres. The labels and the iron atoms shown in black are from the SORs from *I. hospitalis* in panel A, *N. equitans* in panel B, and E23A *I. hospitalis* in panel C. The colored labels are from the different SORs presented in each panel according to their color.

similar to those of the equivalent lysines in the SOR protein structures in the "open conformation": Lys15 in *P. furiosus* SOR,[10] Lys16 in *Thermotoga maritima* SOR (PDB entries 2AMU and 3QZB), Lys49 in *Treponema pallidum* SOR,[16] Lys47 in *Desulfovibrio desulfuricans* SOR,[58] and Lys48 in *D. baarsii* SOR[14,15] (Figure 4B). In chain C of the *N. equitans* SOR crystal structure, a solvent molecule is observed 2.6 Å from the iron and 4.8 Å from the N^{ζ} atom of Lys9 (Table 3). Because the pK_a of this SOR for the $Fe^{3+}-(H_2O)-OH^-$ equilibrium is 6.5,[23] and the protein buffer is at pH 7.2, this solvent molecule is most probably a hydroxide anion, instead of a water molecule.

Although *N. equitans* SOR does not have the canonical glutamate ligand, the hypothesis that Glu5 could be a substitute was previously raised; however, modeling studies and spectroscopic analyses led to the proposal that the binding of Glu5 to the iron was not very likely and that no glutamate residue was bound to the iron in the oxidized state.[23] In fact, analysis of the *N. equitans* SOR structure shows that Glu5 is too far from the iron center, with the carboxyl $O^{\varepsilon 1}$ being at 14 Å from the iron atom. The protein contains other glutamate residues such as Glu32 and Glu38 from the same subunit (e.g., subunit A) or Glu56 from a neighboring antiparallel monomer (e.g., subunit B). However, the distance from these residues to the iron center indicates that they cannot substitute for the canonical glutamate: Glu32 $O^{\varepsilon 2}$ and Glu38 $O^{\varepsilon 1}$ are at ∼15 and ∼9 Å, respectively, from the iron atom in the same subunit (e.g., subunit A), whereas Glu56 $O^{\varepsilon 1}$ from subunit B is ∼9 Å away from the iron atom in subunit A. Nevertheless, analysis of the structure presented here shows that asparagine 7 (Asn7 $O^{\delta 1}$) is at ∼7.2 Å from the iron and is hydrogen-bonded (∼3 Å) to one of the coordinating histidines, His10 $N^{\delta 1}$ (Figure 3D), which was not predicted by the previous modeling studies.[23] Interestingly, this residue is at the same structural position as Glu14 or Glu15 in the "open conformation" crystal structures of *P. furiosus* SOR[10] (PDB entry 1DQK) or *T. maritima* SOR (PDB entry 3QZB), respectively (Figure 4B).

An Alternative Lysine Residue in E23A *I. hospitalis* SOR. As mentioned above, *I. hospitalis* SOR is a "natural mutant", lacking the highly conserved lysine, and therefore, the E23A *I. hospitalis* SOR variant may be viewed as a "double mutant", lacking the glutamate and lysine residues. The crystal structure of E23A *I. hospitalis* SOR revealed that the region between residues Thr10 and Ala23 has a conformation different from that of the wild-type enzyme (Figure 3A). This conformational arrangement is such that the second axial coordinating position is accessible for the binding of solvent molecules. In fact, this was observed on all four molecules in the asymmetric unit (Table 3). Because the pK_a of the $Fe^{3+}-(H_2O)-OH^-$ equilibrium is 6.5 for E23A *I. hospitalis* SOR, while for the wild-type SOR it is ∼10.5,[24] at pH 8.5, the value used for protein crystallization, the solvent molecules that were observed coordinating the iron are probably hydroxide anions.

Analysis of the E23A *I. hospitalis* SOR protein structure further revealed that because of the conformational arrangement observed for the N-terminal segment in this mutant, there is a "nonstandard" lysine residue close to the iron center, Lys21, whose N^{ξ} is at ∼6 Å from the iron (Figure 3C and Table 3). In the amino acid sequences, this lysine is located before the glutamate of the -(E)(K)HVP- motif (Figure 2) and is also quite well conserved, not only in enzymes lacking the canonical lysine[24] but also in other SORs that contain that residue, such as those from *P. furiosus* (Lys12), *P. horikoshii* (Lys21), and *T. maritima* (Lys13) (Figure 2). The structural position of lysine 21 in the wild-type *I. hospitalis* SOR is comparable with those of Lys12 in *P. furiosus* (1DO6, chain A; 1DQI, chain A) and Lys21 in *P. horikoshii* (2HVB, chain D) SORs (Figure 4A). Remarkably, in the E23A mutant, the position of that Lys21 relative to the iron center is completely different from those of the canonical lysines in the "open

DOI: 10.1021/acs.biochem.8b00334
Biochemistry 2018, 57, 5271−5281

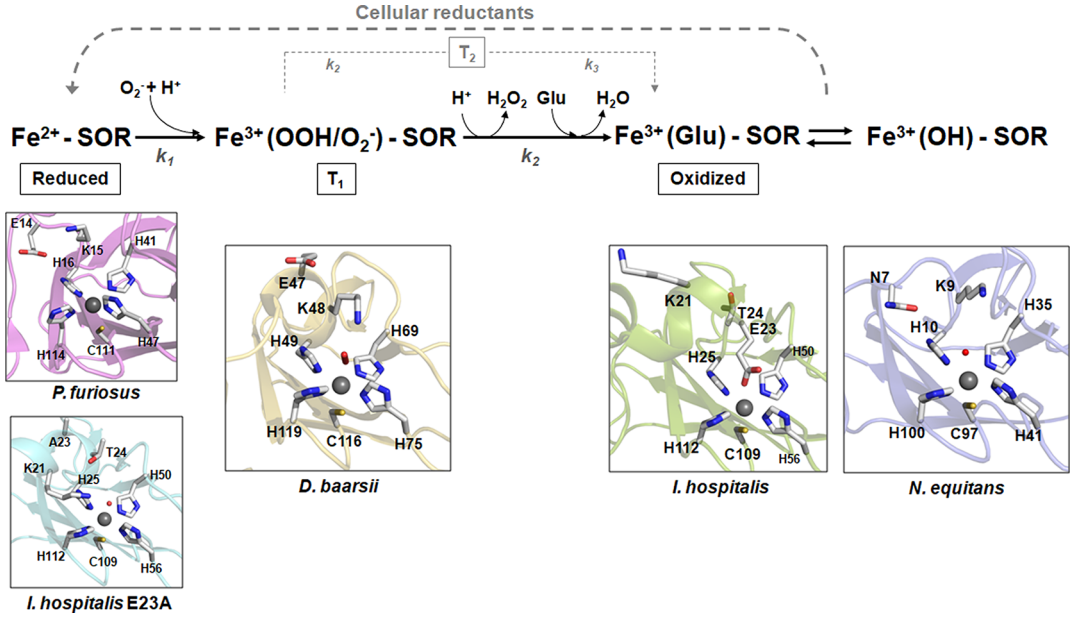

Figure 5. Structural view of the SOR catalytic mechanism. The reduced state corresponds to the center in the ferrous state that is ready to receive the superoxide anion, represented by the *P. furiosus* SOR (1DQK, chain C)[10] and E23A *I. hospitalis* SOR (chain A) structures. The T1 intermediate state corresponds to the ferric hydroperoxide species that is stabilized by the positively charged lysine; this state is represented by the structure of *D. baarsii* SOR (2JI3, chain B) where an iron-bound peroxo species was observed.[15] In the T2 intermediate state, a hydroxide molecule is bound to the iron in the ferric state. In the case of *N. equitans* SOR and E23A *I. hospitalis* SOR, this is the final sate. The oxidized state corresponds to the binding of glutamate to the iron atom, represented by the structures from *I. hospitalis* SOR (chain A) and *N. equitans* SOR in the basic form.

conformation" such as the crystal structure of *P. furiosus* SOR, as illustrated in Figure 4C, but is close to the iron ion. Therefore, the role of Lys21 in *I. hospitalis* SOR is most likely equivalent to that of the canonical lysines, stabilizing and acting as a proton donor to catalytic intermediates, thus explaining why the catalytic kinetics of *I. hospitalis* SOR is similar to those of proteins with the canonical lysine.[24]

Structural Mechanism of the Catalytic Reaction. The SOR mechanism for reducing superoxide has been reviewed in refs 2 and 5. Briefly, the cycle starts with the enzyme in the ferrous state, in the "open conformation". Once superoxide binds, a possible Fe(II)−superoxo state is formed (whose detection, or not, is still a matter of dispute; cf. ref 59 for the most recent discussion), which, if formed, decays rapidly to an iron (hydro)peroxo species (T1 state[59]) and then to the oxidized closed form when the glutamate is present; for some enzymes, a third intermediate is detected, assigned to a ferric−hydroxo species (T2), which subsequently transforms in a first-order process into the oxidized resting state.[15,18,21,22,60−65] The cycle is completed by reduction of the iron center by the action of cellular reductants.[62,66−68] It has been shown that upon iron reduction SORs undergo a redox-driven structural change, as observed by FTIR and X-ray studies.[4,10,12,13] Analyzing all the available SOR structures together with those presented here, we are able to structurally represent most states of the catalytic mechanism, for 1Fe- and 2Fe-SORs (Figure 5). As mentioned above, the catalytic cycle starts with the protein in the "open conformation" state, in which the iron atom is in the ferrous form. Thus, the initial state (reduced) can be represented by the structure of the reduced SOR from *P. furiosus*, for the canonical enzymes, or the E23A *I. hospitalis* SOR, for the lysine-lacking enzymes.

Although in the latter the iron is in the ferric form, this structure should be similar to that of the reduced state, because it lacks the glutamate residue and FTIR studies of E23A *I. hospitalis* SOR did not reveal significant structural changes upon iron reduction;[12] this suggests that the E23A *I. hospitalis* SOR structure would be similar in the oxidized and reduced states, therefore mimicking also the initial state. In this state, Lys21 (*I. hospitalis* SOR) or Lys15 (*P. furiosus* SOR) is pointing toward the iron and ready to stabilize the anionic substrate molecule that will bind to the vacant axial position. In the next step of the catalytic cycle, the first detectable intermediate is formed, corresponding to the T1 intermediate state proposed to be a ferric iron−hydroperoxide (Fe^{3+}−OOH) species.[59] Structurally, this state may be represented by the crystal structure of the iron−peroxide intermediate of the E114A mutant of *D. baarsii* SOR (PDB entry 2JI3) in which a peroxo molecule is bound to the iron, at a distance of 2.00 Å, and is stabilized by the N^{ζ} atom of the conserved lysine residue (*D. baarsii* SOR Lys48) at a distance of 2.74 Å.[15] Upon release of the product, the lysine moves away, together with the stretch of amino acids (from Gly9 to Lys15 in *P. furiosus*) that contains the glutamate (if present), previously far from the ferric site, which then occupies the vacant iron sixth coordination position. Therefore, in the glutamate-containing SORs, the oxidized state is represented by the structure of *I. hospitalis* SOR, where the glutamate is bound in a monodentate mode to the iron at a distance of ∼2.5 Å, like in other SORs, such as those from *P. furiosus* and *G. intestinalis*. The *N. equitans* SOR (chain A) structure represents the oxidized states in the basic form, because this protein has a pK_a in the oxidized form of 6.5;[23] in this form, a hydroxide anion, as mentioned above, is at 2.6 Å from the iron and 4.8 Å from Lys9 (N^{ζ}) (Table 3 and Figure 5). This form also corresponds most probably to intermediate T2 detected in *Archaeoglobus fulgidus* and *D. baarsii* SORs,[22,62] assigned also to a ferric Fe−hydroxide-bound species. The structural change in the region containing the -(E)(K)HxP- motif is indeed not only redox-driven but also pH-driven.

DOI: 10.1021/acs.biochem.8b00334
Biochemistry 2018, 57, 5271−5281

CONCLUSIONS

Superoxide reductases (SORs) are enzymes involved in the reduction of superoxide to hydrogen peroxide, an enzymatic system present in anaerobic or aerobic organisms from the three domains of life. The hyperthermophilic and symbiotic archaea *I. hospitalis* and *N. equitans* rely only on this type of protein to perform the detoxification of the superoxide anion radical. Several studies have been performed over the years to characterize the catalytic mechanism of these enzymes, and from these studies, two residues were proposed to play a crucial role in the catalytic mechanism, the glutamate and the lysine from the -(E)(K)HxP- binding motif. To address the role of these two residues, we have conducted a structural characterization of the two SORs from *I. hospitalis* and *N. equitans*, which can be regarded as two natural mutants: *N. equitans* SOR lacks the active site gatekeeper glutamate, while *I. hospitalis* SOR does not have the adjacent conserved lysine that has been proposed to stabilize the anionic molecule bound to the iron, the superoxide, or the hydroperoxide anions. Furthermore, to complement our studies, the structure of one site-directed *I. hospitalis* SOR mutant was also determined and analyzed, E23A *I. hospitalis* SOR, representing a double mutant missing both canonical glutamate and lysine residues.

Although the structural architectures of the monomers and the quaternary structures are very similar for the presented structures, the analyses of the iron catalytic center environment show striking differences that may represent different kinetic states. On the basis of this and previous structural information from SORs, we propose a model like a "structural movie" for the superoxide reduction by superoxide reductases, which includes an alternative catalytically important lysine residue for the *I. hospitalis* and related SORs.

AUTHOR INFORMATION

Corresponding Authors

*Instituto de Biologia Experimental e Tecnológica, Apartado 12, 2781-901 Oeiras, Portugal. Telephone: +351 214469462. Fax: +351 214421161. E-mail: tiagob@itqb.unl.pt.

*ITQB NOVA, Instituto de Tecnologia Química e Biológica António Xavier, Universidade Nova de Lisboa, Av. da República, 2780-157 Oeiras, Portugal. Telephone: +351 214469322. Fax: +351 214411277. E-mail: miguel@itqb.unl.pt.

*ITQB NOVA, Instituto de Tecnologia Quimica e Biológica António Xavier, Universidade Nova de Lisboa, Av. da República, 2780-157 Oeiras, Portugal. Telephone: +351 214469665. Fax: +351 214411277. E-mail: cmromao@itqb.unl.pt.

ORCID

Célia V. Romão: 0000-0002-9474-2405

Author Contributions

C.V.R., P.M.M., M.T., and T.M.B. planned the project. C.V.R., C.M.S., F.G.P., A.F.P., T.M.B., and P.M.M. performed experiments covering protein purification (C.V.R., C.M.S., and A.F.P.), protein crystallization (C.M.S., F.G.P., and T.M.B.), and determination of protein structure and refinement (P.M.M., C.M.S., F.G.P., and T.M.B.). C.V.R., P.M.M., C.M.S., M.T., and T.M.B. analyzed data and wrote the manuscript.

Funding

This work was financed by Fundação para a Ciência e Tecnologia (FCT) through Projects PTDC/BIA-PRO/111940/2009 (T.M.B.) and PTDC/BBB-BQB/3135/2014 (M.T.). This work was further financially supported by Project LISBOA-01-0145-FEDER-007660 (Microbiologia Molecular, Estrutural e Celular-MostMicro) funded by FEDER funds through COMPETE2020-Programa Operacional Competitividade e Internacionalização (POCI) and by national funds through FCT-Fundação para a Ciência e a Tecnologia, and by the iNOVA4Health Research Unit (LISBOA-01-0145-FEDER-007344), which is co-funded by Fundação para a Ciência e Tecnologia/Ministério da Ciência e do Ensino Superior, through national funds, and by FEDER under the PT2020 Partnership Agreement. C.M.S. was supported by a BI fellowship within FCT Project PTDC/BIA-PRO/111940/2009. F.G.P. was supported by an IBET fellowship. A.F.P. is the recipient of Ph.D. Grant SFRH/BD/41355/2007. C.V.R. is the recipient of Grant SFRH/BPD/94050/2013.

Notes

The authors declare no competing financial interest.

ACKNOWLEDGMENTS

The authors thank the ESRF (Grenoble, France) and the ID23-1 beamline staff for support during the synchrotron data collections.

REFERENCES

(1) Jenney, F. E., Jr., Verhagen, M. F., Cui, X., and Adams, M. W. (1999) Anaerobic microbes: oxygen detoxification without superoxide dismutase. *Science 286*, 306−309.

(2) Sheng, Y., Abreu, I. A., Cabelli, D. E., Maroney, M. J., Miller, A. F., Teixeira, M., and Valentine, J. S. (2014) Superoxide dismutases and superoxide reductases. *Chem. Rev. 114*, 3854−3918.

(3) Bonnot, F., Tremey, E., von Stetten, D., Rat, S., Duval, S., Carpentier, P., Clemancey, M., Desbois, A., and Niviere, V. (2014) Formation of high-valent iron-oxo species in superoxide reductase: characterization by resonance Raman spectroscopy. *Angew. Chem., Int. Ed. 53*, 5926−5930.

(4) Pereira, A. S., Tavares, P., Folgosa, F., Almeida, R. M., Moura, I., and Moura, J. J. G. (2007) Superoxide Reductases. *Eur. J. Inorg. Chem. 2007*, 2569−2581.

(5) Pinto, A. F., Rodrigues, J. V., and Teixeira, M. (2010) Reductive elimination of superoxide: Structure and mechanism of superoxide reductases. *Biochim. Biophys. Acta, Proteins Proteomics 1804*, 285−297.

(6) Chen, L., Sharma, P., Le Gall, J., Mariano, A. M., Teixeira, M., and Xavier, A. V. (1994) A blue non-heme iron protein from *Desulfovibrio gigas*. *Eur. J. Biochem. 226*, 613−618.

(7) Lombard, M., Fontecave, M., Touati, D., and Niviere, V. (2000) Reaction of the desulfoferrodoxin from *Desulfoarculus baarsii* with superoxide anion. Evidence for a superoxide reductase activity. *J. Biol. Chem. 275*, 115−121.

(8) Moura, I., Tavares, P., Moura, J. J., Ravi, N., Huynh, B. H., Liu, M. Y., and LeGall, J. (1990) Purification and characterization of desulfoferrodoxin. A novel protein from *Desulfovibrio desulfuricans* (ATCC 27774) and from *Desulfovibrio vulgaris* (strain Hildenborough) that contains a distorted rubredoxin center and a mononuclear ferrous center. *J. Biol. Chem. 265*, 21596−21602.

(9) Lucchetti-Miganeh, C., Goudenege, D., Thybert, D., Salbert, G., and Barloy-Hubler, F. (2011) SORGOdb: Superoxide Reductase Gene Ontology curated DataBase. *BMC Microbiol. 11*, 105.

(10) Yeh, A. P., Hu, Y., Jenney, F. E., Jr., Adams, M. W., and Rees, D. C. (2000) Structures of the superoxide reductase from *Pyrococcus furiosus* in the oxidized and reduced states. *Biochemistry 39*, 2499−2508.

(11) Sousa, C. M., Carpentier, P., Matias, P. M., Testa, F., Pinho, F., Sarti, P., Giuffre, A., Bandeiras, T. M., and Romao, C. V. (2015) Superoxide reductase from *Giardia intestinalis*: structural characterization of the first SOR from a eukaryotic organism shows an iron

DOI: 10.1021/acs.biochem.8b00334
Biochemistry 2018, 57, 5271−5281

centre that is highly sensitive to photoreduction. *Acta Crystallogr., Sect. D: Biol. Crystallogr. 71*, 2236−2247.
(12) Horch, M., Pinto, A. F., Utesch, T., Mroginski, M. A., Romao, C. V., Teixeira, M., Hildebrandt, P., and Zebger, I. (2014) Reductive activation and structural rearrangement in superoxide reductase: a combined infrared spectroscopic and computational study. *Phys. Chem. Chem. Phys. 16*, 14220−14230.
(13) Berthomieu, C., Dupeyrat, F., Fontecave, M., Vermeglio, A., and Niviere, V. (2002) Redox-dependent structural changes in the superoxide reductase from *Desulfoarculus baarsii* and *Treponema pallidum*: a FTIR study. *Biochemistry 41*, 10360−10368.
(14) Adam, V., Royant, A., Niviere, V., Molina-Heredia, F. P., and Bourgeois, D. (2004) Structure of superoxide reductase bound to ferrocyanide and active site expansion upon X-ray-induced photoreduction. *Structure 12*, 1729−1740.
(15) Katona, G., Carpentier, P., Niviere, V., Amara, P., Adam, V., Ohana, J., Tsanov, N., and Bourgeois, D. (2007) Raman-assisted crystallography reveals end-on peroxide intermediates in a nonheme iron enzyme. *Science 316*, 449−453.
(16) Santos-Silva, T., Trincao, J., Carvalho, A. L., Bonifacio, C., Auchere, F., Raleiras, P., Moura, I., Moura, J. J., and Romao, M. J. (2006) The first crystal structure of class III superoxide reductase from *Treponema pallidum*. *JBIC, J. Biol. Inorg. Chem. 11*, 548−558.
(17) Lombard, M., Houee-Levin, C., Touati, D., Fontecave, M., and Niviere, V. (2001) Superoxide reductase from *Desulfoarculus baarsii*: reaction mechanism and role of glutamate 47 and lysine 48 in catalysis. *Biochemistry 40*, 5032−5040.
(18) Mathe, C., Mattioli, T. A., Horner, O., Lombard, M., Latour, J. M., Fontecave, M., and Niviere, V. (2002) Identification of iron(III) peroxo species in the active site of the superoxide reductase SOR from *Desulfoarculus baarsii*. *J. Am. Chem. Soc. 124*, 4966−4967.
(19) David, R., Jamet, H., Niviere, V., Moreau, Y., and Milet, A. (2017) Iron Hydroperoxide Intermediate in Superoxide Reductase: Protonation or Dissociation First? MM Dynamics and QM/MM Metadynamics Study. *J. Chem. Theory Comput. 13*, 2987−3004.
(20) Abreu, I. A., Saraiva, L. M., Soares, C. M., Teixeira, M., and Cabelli, D. E. (2001) The mechanism of superoxide scavenging by *Archaeoglobus fulgidus* neelaredoxin. *J. Biol. Chem. 276*, 38995−39001.
(21) Emerson, J. P., Coulter, E. D., Cabelli, D. E., Phillips, R. S., and Kurtz, D. M., Jr (2002) Kinetics and mechanism of superoxide reduction by two-iron superoxide reductase from *Desulfovibrio vulgaris*. *Biochemistry 41*, 4348−4357.
(22) Bonnot, F., Molle, T., Menage, S., Moreau, Y., Duval, S., Favaudon, V., Houee-Levin, C., and Niviere, V. (2012) Control of the evolution of iron peroxide intermediate in superoxide reductase from *Desulfoarculus baarsii*. Involvement of lysine 48 in protonation. *J. Am. Chem. Soc. 134*, 5120−5130.
(23) Rodrigues, J. V., Victor, B. L., Huber, H., Saraiva, L. M., Soares, C. M., Cabelli, D. E., and Teixeira, M. (2008) Superoxide reduction by *Nanoarchaeum equitans* neelaredoxin, an enzyme lacking the highly conserved glutamate iron ligand. *JBIC, J. Biol. Inorg. Chem. 13*, 219−228.
(24) Pinto, A. F., Romao, C. V., Pinto, L. C., Huber, H., Saraiva, L. M., Todorovic, S., Cabelli, D., and Teixeira, M. (2015) Superoxide reduction by a superoxide reductase lacking the highly conserved lysine residue. *JBIC, J. Biol. Inorg. Chem. 20*, 155−164.
(25) Huber, H., Hohn, M. J., Rachel, R., Fuchs, T., Wimmer, V. C., and Stetter, K. O. (2002) A new phylum of Archaea represented by a nanosized hyperthermophilic symbiont. *Nature 417*, 63−67.
(26) Pinho, F. G., Pinto, A. F., Pinto, L. C., Huber, H., Romao, C. V., Teixeira, M., Matias, P. M., and Bandeiras, T. M. (2011) Superoxide reductase from *Nanoarchaeum equitans*: expression, purification, crystallization and preliminary X-ray crystallographic analysis. *Acta Crystallogr., Sect. F: Struct. Biol. Cryst. Commun. 67*, 591−595.
(27) Pinho, F. G., Romao, C. V., Pinto, A. F., Saraiva, L. M., Huber, H., Matias, P. M., Teixeira, M., and Bandeiras, T. M. (2010) Cloning, purification, crystallization and X-ray crystallographic analysis of *Ignicoccus hospitalis* neelaredoxin. *Acta Crystallogr., Sect. F: Struct. Biol. Cryst. Commun. 66*, 605−607.
(28) Kabsch, W. (1993) Automatic Processing of Rotation Diffraction Data from Crystals of Initially Unknown Symmetry and Cell Constants. *J. Appl. Crystallogr. 26*, 795−800.
(29) Winn, M. D., Ballard, C. C., Cowtan, K. D., Dodson, E. J., Emsley, P., Evans, P. R., Keegan, R. M., Krissinel, E. B., Leslie, A. G., McCoy, A., McNicholas, S. J., Murshudov, G. N., Pannu, N. S., Potterton, E. A., Powell, H. R., Read, R. J., Vagin, A., and Wilson, K. S. (2011) Overview of the CCP4 suite and current developments. *Acta Crystallogr., Sect. D: Biol. Crystallogr. 67*, 235−242.
(30) Pape, T., and Schneider, T. R. (2004) HKL2MAP: a graphical user interface for macromolecular phasing with SHELX programs. *J. Appl. Crystallogr. 37*, 843−844.
(31) Schneider, T. R., and Sheldrick, G. M. (2002) Substructure solution with SHELXD. *Acta Crystallogr., Sect. D: Biol. Crystallogr. 58*, 1772−1779.
(32) Sheldrick, G. M. (2002) Macromolecular phasing with SHELXE. *Z. Kristallogr. - Cryst. Mater. 217*, 644.
(33) Sheldrick, G. M. (2010) Experimental phasing with SHELXC/D/E: combining chain tracing with density modification. *Acta Crystallogr., Sect. D: Biol. Crystallogr. 66*, 479−485.
(34) Vonrhein, C., Blanc, E., Roversi, P., and Bricogne, G. (2006) Automated structure solution with autoSHARP. *Methods Mol. Biol. 364*, 215−230.
(35) Abrahams, J. P., and Leslie, A. G. W. (1996) Methods used in the structure determination of bovine mitochondrial F-1 ATPase. *Acta Crystallogr., Sect. D: Biol. Crystallogr. 52*, 30−42.
(36) Cowtan, K. (1994) dm: an automated procedure for phase improvement by density modication. In *Joint CCP4 and ESF-EACBM Newsletter on Protein Crystallography*, pp 34−48, SERC Daresbury Laboratory, Warrington, U.K.
(37) Brunger, A. T. (1992) Free R value: a novel statistical quantity for assessing the accuracy of crystal structures. *Nature 355*, 472−475.
(38) Murshudov, G. N., Vagin, A. A., and Dodson, E. J. (1997) Refinement of macromolecular structures by the maximum-likelihood method. *Acta Crystallogr., Sect. D: Biol. Crystallogr. 53*, 240−255.
(39) Vagin, A. A., Steiner, R. A., Lebedev, A. A., Potterton, L., McNicholas, S., Long, F., and Murshudov, G. N. (2004) REFMAC5 dictionary: organization of prior chemical knowledge and guidelines for its use. *Acta Crystallogr., Sect. D: Biol. Crystallogr. 60*, 2184−2195.
(40) Cowtan, K. (2006) The Buccaneer software for automated model building. 1. Tracing protein chains. *Acta Crystallogr., Sect. D: Biol. Crystallogr. 62*, 1002−1011.
(41) Emsley, P., and Cowtan, K. (2004) Coot: model-building tools for molecular graphics. *Acta Crystallogr., Sect. D: Biol. Crystallogr. 60*, 2126−2132.
(42) McCoy, A. J., Grosse-Kunstleve, R. W., Storoni, L. C., and Read, R. J. (2005) Likelihood-enhanced fast translation functions. *Acta Crystallogr., Sect. D: Biol. Crystallogr. 61*, 458−464.
(43) Adams, P. D., Afonine, P. V., Bunkoczi, G., Chen, V. B., Davis, I. W., Echols, N., Headd, J. J., Hung, L. W., Kapral, G. J., Grosse-Kunstleve, R. W., McCoy, A. J., Moriarty, N. W., Oeffner, R., Read, R. J., Richardson, D. C., Richardson, J. S., Terwilliger, T. C., and Zwart, P. H. (2010) PHENIX: a comprehensive Python-based system for macromolecular structure solution. *Acta Crystallogr., Sect. D: Biol. Crystallogr. 66*, 213−221.
(44) Winn, M. D., Isupov, M. N., and Murshudov, G. N. (2001) Use of TLS parameters to model anisotropic displacements in macromolecular refinement. *Acta Crystallogr., Sect. D: Biol. Crystallogr. 57*, 122−133.
(45) Chen, V. B., Arendall, W. B., 3rd, Headd, J. J., Keedy, D. A., Immormino, R. M., Kapral, G. J., Murray, L. W., Richardson, J. S., and Richardson, D. C. (2010) MolProbity: all-atom structure validation for macromolecular crystallography. *Acta Crystallogr., Sect. D: Biol. Crystallogr. 66*, 12−21.
(46) Ramachandran, G. N., and Sasisekharan, V. (1968) Conformation of polypeptides and proteins. *Adv. Protein Chem. 23*, 283−438.
(47) Thompson, J. D., Gibson, T. J., Plewniak, F., Jeanmougin, F., and Higgins, D. G. (1997) The CLUSTAL X windows interface:

DOI: 10.1021/acs.biochem.8b00334
Biochemistry 2018, 57, 5271−5281

flexible strategies for multiple sequence alignment aided by quality analysis tools. *Nucleic Acids Res. 25*, 4876−4882.
(48) Painter, J., and Merritt, E. A. (2006) Optimal description of a protein structure in terms of multiple groups undergoing TLS motion. *Acta Crystallogr., Sect. D: Biol. Crystallogr. 62*, 439−450.
(49) Painter, J., and Merritt, E. A. (2006) TLSMD web server for the generation of multi-group TLS models. *J. Appl. Crystallogr. 39*, 109−111.
(50) Webb, B., and Sali, A. (2014) Protein structure modeling with MODELLER. *Methods Mol. Biol. 1137*, 1−15.
(51) Nicholas, K. B., Nicholas, H. B., and Deerfield, D. W. (1997) GeneDoc: Analysis and Visualization of Genetic Variation. In *EMBNEW NEWS*, p 14.
(52) DeLano, W. L. (2002) *The PyMOL Molecular Graphics System*, DeLano Scientific, San Carlos, CA.
(53) *PyMOL Molecular Graphics System*, version 1.3r1 (2010) Schrodinger, LLC.
(54) Velankar, S., Alhroub, Y., Alili, A., Best, C., Boutselakis, H. C., Caboche, S., Conroy, M. J., Dana, J. M., van Ginkel, G., Golovin, A., Gore, S. P., Gutmanas, A., Haslam, P., Hirshberg, M., John, M., Lagerstedt, I., Mir, S., Newman, L. E., Oldfield, T. J., Penkett, C. J., Pineda-Castillo, J., Rinaldi, L., Sahni, G., Sawka, G., Sen, S., Slowley, R., Sousa da Silva, A. W., Suarez-Uruena, A., Swaminathan, G. J., Symmons, M. F., Vranken, W. F., Wainwright, M., and Kleywegt, G. J. (2011) PDBe: Protein Data Bank in Europe. *Nucleic Acids Res. 39*, D402−410.
(55) Velankar, S., Alhroub, Y., Best, C., Caboche, S., Conroy, M. J., Dana, J. M., Fernandez Montecelo, M. A., van Ginkel, G., Golovin, A., Gore, S. P., Gutmanas, A., Haslam, P., Hendrickx, P. M., Heuson, E., Hirshberg, M., John, M., Lagerstedt, I., Mir, S., Newman, L. E., Oldfield, T. J., Patwardhan, A., Rinaldi, L., Sahni, G., Sanz-Garcia, E., Sen, S., Slowley, R., Suarez-Uruena, A., Swaminathan, G. J., Symmons, M. F., Vranken, W. F., Wainwright, M., and Kleywegt, G. J. (2012) PDBe: Protein Data Bank in Europe. *Nucleic Acids Res. 40*, D445−452.
(56) Krissinel, E., and Henrick, K. (2007) Inference of macromolecular assemblies from crystalline state. *J. Mol. Biol. 372*, 774−797.
(57) McDonald, I. K., and Thornton, J. M. (1994) Satisfying hydrogen bonding potential in proteins. *J. Mol. Biol. 238*, 777−793.
(58) Coelho, A. V., Matias, P., Fulõp, V., Thompson, A., Gonzalez, A., and Carrondo, M. A. (1997) Desulfoferrodoxin Structure Determined by MAD Phasing and Refinement to 1.9 Angstroms Resolution Reveals a Unique Combination of a Tetrahedral FeS4 Centre with a Square Pyramidal FeSn4 Centre. *JBIC, J. Biol. Inorg. Chem. 2*, 680−689.
(59) Attia, A. A., Cioloboc, D., Lupan, A., and Silaghi-Dumitrescu, R. (2016) Multiconfigurational and DFT analyses of the electromeric formulation and UV-vis absorption spectra of the superoxide adduct of ferrous superoxide reductase. *J. Inorg. Biochem. 165*, 49−53.
(60) Bonnot, F., Houee-Levin, C., Favaudon, V., and Niviere, V. (2010) Photochemical processes observed during the reaction of superoxide reductase from *Desulfoarculus baarsii* with superoxide: re-evaluation of the reaction mechanism. *Biochim. Biophys. Acta, Proteins Proteomics 1804*, 762−767.
(61) Rodrigues, J. V., Abreu, I. A., Cabelli, D., and Teixeira, M. (2006) Superoxide reduction mechanism of *Archaeoglobus fulgidus* one-iron superoxide reductase. *Biochemistry 45*, 9266−9278.
(62) Rodrigues, J. V., Saraiva, L. M., Abreu, I. A., Teixeira, M., and Cabelli, D. E. (2007) Superoxide reduction by *Archaeoglobus fulgidus* desulfoferrodoxin: comparison with neelaredoxin. *JBIC, J. Biol. Inorg. Chem. 12*, 248−256.
(63) Mathe, C., Niviere, V., Houee-Levin, C., and Mattioli, T. A. (2006) Fe(3+)-eta(2)-peroxo species in superoxide reductase from *Treponema pallidum*. Comparison with *Desulfoarculus baarsii*. *Biophys. Chem. 119*, 38−48.
(64) Silaghi-Dumitrescu, R., Silaghi-Dumitrescu, I., Coulter, E. D., and Kurtz, D. M., Jr (2003) Computational study of the non-heme iron active site in superoxide reductase and its reaction with superoxide. *Inorg. Chem. 42*, 446−456.
(65) Testa, F., Mastronicola, D., Cabelli, D. E., Bordi, E., Pucillo, L. P., Sarti, P., Saraiva, L. M., Giuffre, A., and Teixeira, M. (2011) The superoxide reductase from the early diverging eukaryote *Giardia intestinalis*. *Free Radical Biol. Med. 51*, 1567−1574.
(66) Auchere, F., Sikkink, R., Cordas, C., Raleiras, P., Tavares, P., Moura, I., and Moura, J. J. (2004) Overexpression and purification of *Treponema pallidum* rubredoxin; kinetic evidence for a superoxide-mediated electron transfer with the superoxide reductase neelaredoxin. *JBIC, J. Biol. Inorg. Chem. 9*, 839−849.
(67) Emerson, J. P., Coulter, E. D., Phillips, R. S., and Kurtz, D. M., Jr (2003) Kinetics of the superoxide reductase catalytic cycle. *J. Biol. Chem. 278*, 39662−39668.
(68) Rodrigues, J. V., Abreu, I. A., Saraiva, L. M., and Teixeira, M. (2005) Rubredoxin acts as an electron donor for neelaredoxin in *Archaeoglobus fulgidus*. *Biochem. Biophys. Res. Commun. 329*, 1300−1305.
(69) Weiss, M. S. (2001) Global indicators of X-ray data quality. *J. Appl. Crystallogr. 34*, 130−135.

DOI: 10.1021/acs.biochem.8b00334
Biochemistry 2018, 57, 5271−5281